Modeling 1D Cold Electrostatic Plasma with a Lagrangian Particle Method

Horacio Moreno Montanes Robert Krasny

July 11, 2023

Abstract

The conventional approach to plasma simulations utilizes the particle-in-cell (PIC) method, but PIC simulations often lose resolution as complex features appear in the evolving plasma. This project develops an alternative Lagrangian particle method for a one-dimensional cold electrostatic plasma with periodic boundary conditions, which is both efficient and preserves accuracy as the plasma evolves in time, in contrast to existing methods. The plasma is described by the Vlasov-Poisson equations for the electron distribution in phase space and the self-consistent electric field in physical space. The plasma is represented by discrete charged macro-particles (representing electrons) with a neutralizing constant background distribution of positively charged ions. Two integration techniques, Euler's method and fourth order Runge-Kutta, are used to evolve the electrons, and regularization is applied to ensure continuity of the electric field. We investigate the effect of the numerical parameters, including the time step Δt, number of particles N, and the regularization parameter δ. Initial results indicate that the lack of continuity in the non-regularized problem contributes to error growth for both integration schemes. Additionally, a particle insertion scheme is implemented to preserve the resolution of the plasma. Future extensions of this work seek to apply the method to study other distributions, like the two-stream instability and warm distributions, and further investigate the effects of electric field regularization regarding energy conservation and charge transport.

Contents

1 Introduction

Plasma, characterized by their ionized state and collective behavior, exhibit a wide range of phenomena with applications in various fields, including particle acceleration, ion beams, fusion, and plasma physics. Accurate modeling of plasma dynamics is essential for understanding and predicting their complex behavior. While the particle-in-cell (PIC) methods have been a widely employed approach, they can suffer from resolution loss as plasma evolves and develops intricate features. Other methods have been developed to improve on some of the shortcomings of PIC methods such as grid instability and numerical heating, however these methods also tend to lose definition [Mit+19]. In this study, we explore an alternative Lagrangian particle method for modeling a one-dimensional cold, electrostatic plasma with periodic boundary conditions, aiming to overcome the resolution limitations observed in conventional approaches.

The governing equations for our plasma model are the Vlasov-Poisson equations, which encapsulate the charge conservation and plasma behavior due to the self-consistent electrostatic forces:

$$\partial_t f + v\partial_x f + F\partial_v f = 0 \quad F = qE \quad E = -\partial_x \varphi \quad -\partial_x^2 \varphi = \rho, \tag{1}$$

where $f(x, v, t)$ is the particle number distribution in phase space, $F(x, t)$ is the electrostatic force, $E(x, t)$ is the electric field, $\varphi(x, t)$ is the electric potential and $\rho(x, t)$ is the charge density. The Vlasov equation describes the evolution of the plasma distribution in phase space, considering the interplay between particle trajectories and the collective electric field. Meanwhile, the Poisson equation governs the dynamics of the self-consistent electric field, influenced by the charge distribution within the plasma.

The primary objective of this paper is to develop an efficient modeling method that preserves resolution as the plasma evolves in time. This method is tested on simplest case: a one-dimensional cold, electrostatic plasma, as a proof of concept. To evolve the plasma in time and address the resolution challenges, we employ a Lagrangian approach coupled with discrete charged particles (representing packets of electrons) and a neutralizing background distribution of positively charged ions that incorporates an adaptive particle insertion scheme. This method approximates the exact solution to the Vlasov-Poisson equations, which can be obtained through an integral expression related to the Green's function for the 1D Laplace operator, rather than employing finite difference schemes. This allows for flexibility in the degree of resolution for approximate solution within specific intervals, enabling the preservation of detail where necessary without imposing excessive computational demands. Two integration techniques, namely Euler's method and the fourth-order Runge-Kutta (RK4) scheme, are employed to numerically evolve the electrons. While both methods are used for comparison, the RK4 scheme is favored due to its higher accuracy. An additional parameter in introduced to smooth out discontinuities in the resulting electric field, and its effects on the overall evolution of the plasma are investigated. Finally, the method is improved by the introduction of an adaptive particle insertion scheme that helps preserve definition as the plasma evolves.

In addition to this, we envision extending this Lagrangian particle method to different distributions such as several streams and warm plasma distributions with continuous velocity profiles, enabling its application to a broader range of plasma distributions and phenomena. Overall, this research provides insights into a promising alternative approach for plasma simulations, offering improved resolution and accuracy compared to conventional methods. By developing a Lagrangian particle method for plasma modeling, we contribute to the advancement of plasma physics and its applications across various disciplines.

2 Formulation

2.1 Derivation of the Electric Potential and Electric Field

For this problem, we consider the Poisson equation in Eq. (1), subject to periodic boundary conditions on the interval $0 \leqslant x \leqslant 1$, with charge density given by

$$\rho(x, t) = q \int_{-\infty}^{\infty} f(x, v, t) dv + 1 \tag{2}$$

satisfying charge neutrality

$$\int_0^1 \rho(x, t) dx = 0. \tag{3}$$

We make use of the Green's function for the 1D Laplace operator, given by

$$g(x,y) = -\frac{1}{2}|x-y| \tag{4}$$

to construct a solution for the potential $\varphi(x,t)$ of the form

$$\varphi(x,t) = ax + b + \int_0^1 g(x,y)\rho(y,t)dy \tag{5}$$

As shown by Sandberg et al., [STK23], after applying charge neutality as well as boundary conditions, we arrive at expressions for the electric potential φ and electric field E given by

$$\varphi(x,t) = \int_0^1 (g(x,y) - xy)\rho(y,t)dy \quad E(x,t) = \int_{-\infty}^{\infty}\int_0^1 K(x,y)f(y,v,t)dydv \tag{6}$$

where $K(x,y)$ is a kernel function, given by the following expression:

$$K(x,y) = -\frac{1}{2}\text{sign}(x-y) + x - y, \quad 0 \leqslant x,y \leqslant 1. \tag{7}$$

It is important to note that this kernel function $K(x,y)$ gives the electrostatic interactions between two particles, with positions x and y respectively. Therefore, this kernel is somewhat analogous to the electric field at x from a particle at y and vice versa.

2.2 Flow Map

Given a particle with Lagrangian coordinates (α,β) in phase space, the flow map for position and velocity in phase space at time t is denoted $x(\alpha,\beta,t), v(\alpha,\beta,t)$. For this problem, we consider the plasma to have all particles starting with zero velocity, therefore particles are identified using a single Lagrangian coordinate in phase space α with $0 \leqslant \alpha < 1$. Then, the equations that describe the evolution of the particle with coordinate α are given by

$$\partial_t x(\alpha,t) = v(\alpha,t) \quad \partial_t v(\alpha,t) = qE(x(\alpha,t),t) \tag{8}$$

where $E(x,t)$ is the electric field. The interval $[0,1]$ is discretized into N intervals of equal length $1/N$. Then, the Lagrangian coordinate for the i-th particle is given by $\alpha_i = \frac{i-0.5}{N}$ for $i = 1:N$. For ease of notation, let $x_i(t) = x(\alpha_i,t)$, $v_i(t) = v(\alpha_i,t)$ denote the flow map for the particle with coordinate α_i. Then, initial position and velocity of particles is given by

$$x_i(0) = \alpha_i + \varepsilon\sin(2\pi\alpha_i) \quad v_i(0) = 0 \tag{9}$$

where ε is a small perturbation from equilibrium. It should be stated that the Lagrangian coordinates α are chosen such that when $\varepsilon = 0$, the particles are initially positioned at the midpoint of each interval in order to avoid computational issues due to periodicity at the boundaries. Finally, it is important to note that due to the Vlasov equation, the distribution function is invariant in the phase flow. That is,

$$f(x(\alpha,t),v(\alpha,t),t) = f_0(x(\alpha,0),v(\alpha,0)) \tag{10}$$

for some initial distribution f_0.

3 Numerical Methods

3.1 Discretization

The one-dimensional cold plasma distribution is approximated by N particles on a curve in phase space, with initial conditions denoted by Eq. (9). The electric field integral expression in Eq. (6) is discretized and written as

$$E(x,t) = \sum_{j=1}^{N} K(x_i(t),x_j(t))w_j \tag{11}$$

where w_j are respective quadrature weights. Since particles are initially at the midpoints of the intervals in phase space, w_j is given by the length of that particular interval, thus $w_j = 1/N$. As a result of this discretization, we have the equations of motion for particles:

$$x_i''(t) = qE(x_i(t), t) = -\sum_{j=1}^{N} K(x_i(t), x_j(t))w_j. \tag{12}$$

These equations form a system of N 2nd order ODEs. It is important to note that according to the initial conditions outlined in Eq. (9), $0 \leqslant x_i(0) \leqslant 1$ for all $i = 1 : N$. However, as the plasma evolves, some of the particles in phase space may be convected to neighboring intervals. Since periodic boundary conditions are imposed on the spatial dimension of the system, these particles are returned to the interval $[0, 1]$ by replacing x_i with its value modulo 1, as well as keeping track of how many periods they have travelled.

Particle positions and velocities are then updated with either an Euler's method or a fourth order Runge-Kutta (RK4) integration scheme with time step Δt. Even though Euler's method is used to analyze the system and convergence with different time steps Δt, RK4 is favored for most of the results later in the paper due to its greater degree of accuracy.

3.2 Hamiltonian System

Under discretization of the continuous plasma, we have a system of N particles, each with position and velocity functions $x_i(t), v_i(t)$ for $i = 1 : N$. This is a Hamiltonian system, i.e. there exists a function $H(\mathbf{x}, \mathbf{v})$ which is conserved that satisfies

$$\frac{\partial H}{\partial v_i} = x_i' \quad -\frac{\partial H}{\partial x_i} = v_i' \tag{13}$$

for $i = 1 : N$ and $\mathbf{x} = (x_1, x_2, \ldots, x_N)$, $\mathbf{v} = (v_1, v_2, \ldots, v_N)$. In particular, for the case of the non-regularized system with a constant number of particles, the function $H(\mathbf{x}, \mathbf{v})$ is given by

$$H(\mathbf{x}, \mathbf{v}) = \frac{1}{2}\sum_{i=1}^{N} v_i + \frac{1}{2}\sum_{i<j} \left[-|x_i - x_j| + (x_i - x_j)^2\right] w_j \tag{14}$$

where $w_j = w = 1/N$ for all $j = 1 \ldots N$. The Hamiltonian H functions as a measure of energy can be used to assess the accuracy of different integration methods, as well as investigating the effects that the regulation parameters δ introduced later have on the evolution of the system. Furthermore, we can split this quantity into kinetic and potential energies $K(\mathbf{v})$, $U(\mathbf{x})$ as

$$K(\mathbf{v}) = \frac{1}{2}\sum_{i=1}^{N} v_i, \quad U(\mathbf{x}) = \frac{1}{2}\sum_{i<j} \left[-|x_i - x_j| + (x_i - x_j)^2\right] w_j \tag{15}$$

such that $H(\mathbf{x}, \mathbf{v}) = U(\mathbf{x}) + K(\mathbf{v})$.

3.3 Numerical Results

3.3.1 Qualitative Results

Figure 1 illustrates the evolution of a plasma with $N = 128$ particles with time step $\Delta t = 0.01$ and initial perturbation of $\varepsilon = 0.05$ over two periods, each represented with a different color. Additional neighboring periods are also plotted in blue and red. Lines are plotted between particles to show connect neighboring particles and illustrate their overall evolution. It can be seen how the plasma forms a vortex at the center of each period, where the initial perturbation causes density of particles to increase. Figure 1 also shows how on $t = 8$, particles are convected to neighboring periods. At $t = 10$, it can be seen how particles that started towards the edges of each period are transported to opposite edges. This separation of particles causes the plasma to lose definition in areas of lower initial density as it is "stretched", causing the initial connecting lines to cross over the plasma. This behavior can be observed to the extreme in Figure 2, where plots for $t = 10, 15, 20$ show the mixing of the plasma with and without the connecting lines. At this point, it is almost impossible to distinguish the initial plasma periods from each other.

Figure 3 shows how increasing the initial number of particles improves the definition of the plasma after $t = 5$. While this is a possible solution to address the problems shown in Figure 2 by increasing the number of particles towards the edges of each period, it introduces unnecessary detail to other portions of the plasma, which can slow

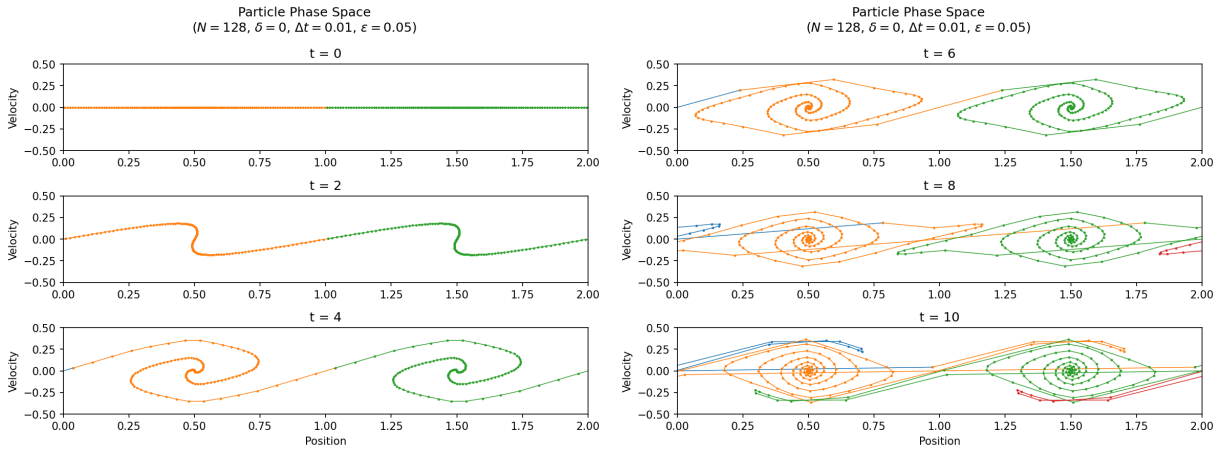

Figure 1: Evolution of plasma with $N = 128$ particles with $\Delta t = 0.01$ subject to initial perturbation of $\varepsilon = 0.05$ (RK4).

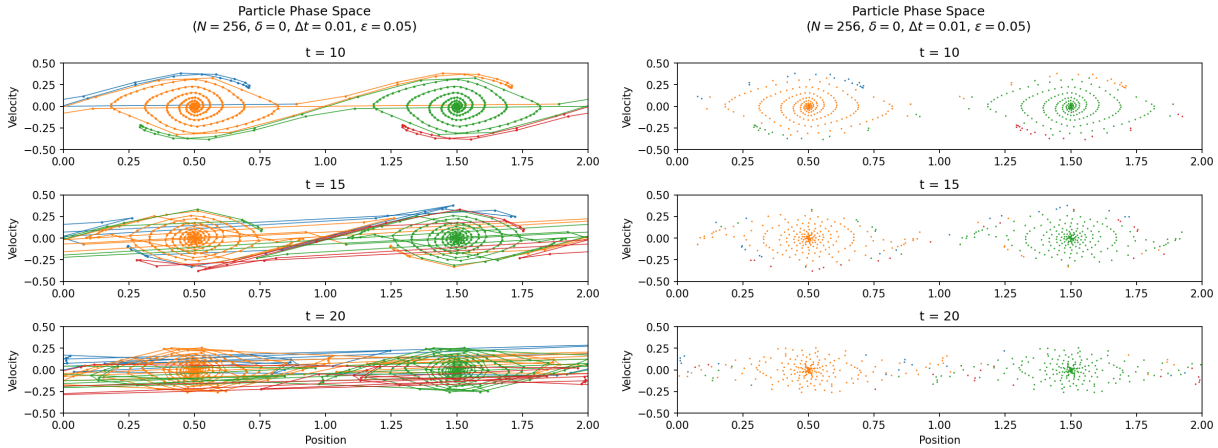

Figure 2: Evolution of plasma for up to $t = 20$ (a) with connecting lines and (b) without connecting lines (RK4).

down computation, especially if detail is needed after longer amounts of time, which will need larger amounts of starting particles. These problems are addressed later on with the introduction of adaptive particle insertion.

Discontinuities in the kernel function in Eq. (7) also cause loss of definition of the plasma, as particles that cross over other particles frequently experience large changes in acceleration for each time step, particularly at the center of the vortices created by the initial perturbations. Figure 4 illustrates these irregularities by zooming into the center of a vorttex in the plasma. Though decreasing the size of time steps is a possible solution, it is also computationally expensive. This problem will be addressed later with the regularization of the electric field.

3.3.2 Error Analysis

Even though all of the previous results were obtained using a fourth-order Runge-Kutta integration scheme, we consider and analyze Euler's method as well to point out some features of this particular problem. These two schemes are evaluated by looking at the energy function in Eq. (13), and it's deviation from the initial quantity. Figure 5a shows the percentage change in error both from Euler's method and RK4. More specifically, the quantitiy plotted is given by the following expression:

$$\%\Delta E = \frac{|H(\mathbf{x}, \mathbf{v}) - H_0|}{H_0} \times 100 \quad H_0 = H(\mathbf{x}(0), \mathbf{v}(0)) \tag{16}$$

In this figure, there are two different time intervals of interest, which can be identified by the drastically different behaviors that both schemes present before and after some time $t = t_c \approx 1.9$. This t_c is the time where a particle first crosses over another particle, breaking the continuity of the ODE in Eq. (12). On the first interval $0 \leqslant t \leqslant t_c$, we can

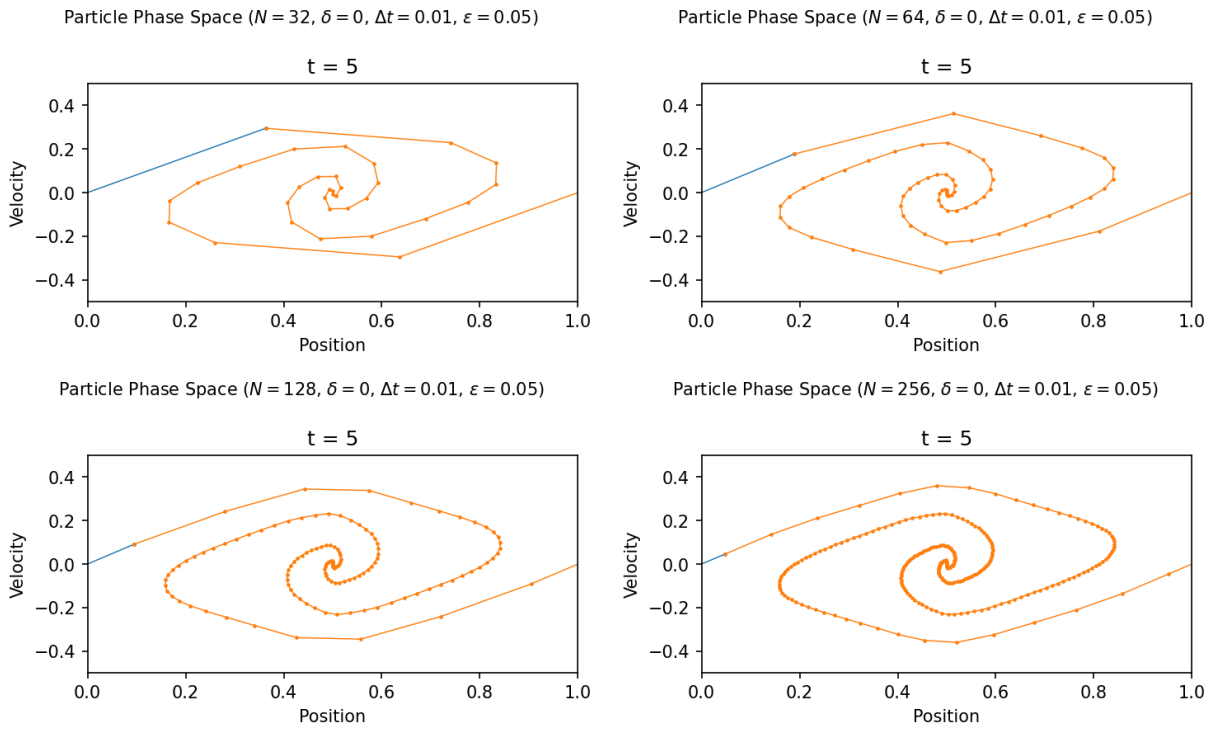

Figure 3: Convergence of plasma at $t = 5$ with fixed $\Delta t = 0.01$ for (a) $N = 32$, (b) $N = 64$, (c) $N = 128$, (d) $N = 256$ using RK4.

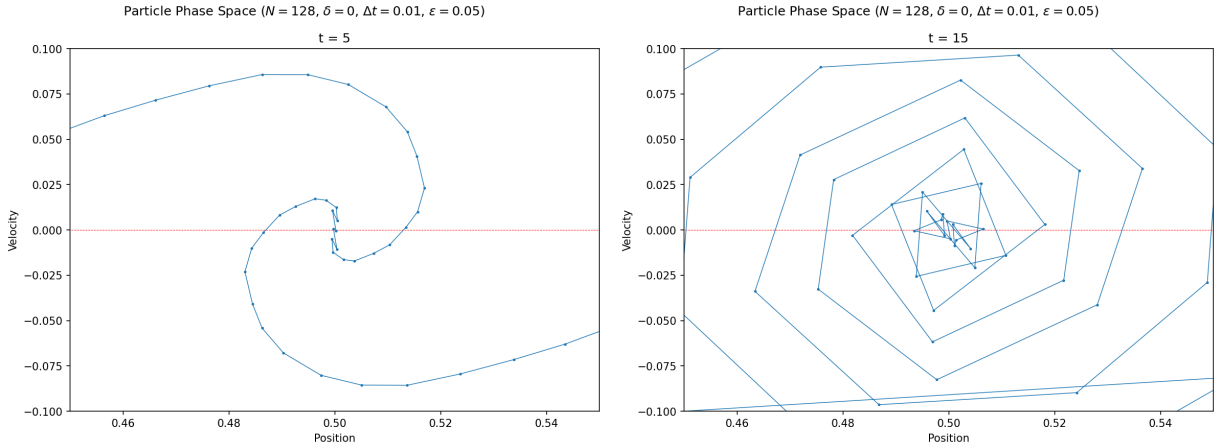

Figure 4: Evolution of the center of the plasma at (a) $t = 5$ and (b) $t = 15$

see how decreasing the time step by a factor of two causes the error to decrease proportionally, as illustrated by the equal differences on a logarithmic scale between each curve for each integration scheme. Additionally, the fact that this difference is larger for RK4 compared to Euler's method shows RK4's higher order of convergence. However, this is no longer the case after $t > t_c$. For Euler's method, there is a sharp increase in the error immediately after $t = t_c$, though it seems like the order of convergence is preserved. RK4 on the other hand, has the deviation from the initial energy oscillating erratically around the order of hundredths of a percent. Though this error seems to be bounded and relatively small, it is no longer the case that decreasing the step size corresponds to a proportional fourth order decrease in the error, due to the loss of continuity of the problem. Still, RK4 achieves results that are orders of magnitude greater than Euler's method in terms of energy.

Figure 5b focuses on the error due to a fixed time step of $\Delta t = 1/32$ for both schemes. Similarly to Eq. 16, these quantities are calculated by:

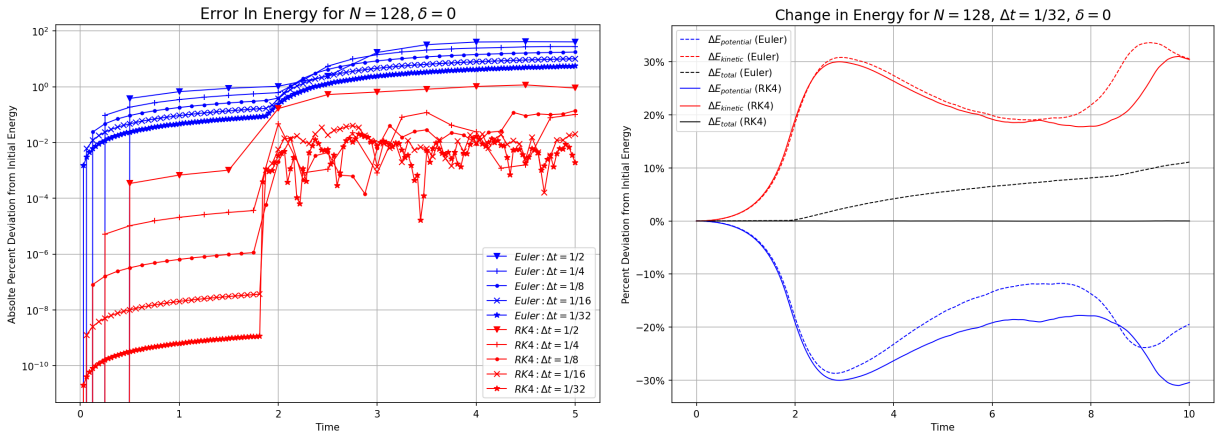

Figure 5: Error analysis for plasma with $N = 128$, $\varepsilon = 0.05$. (a) shows percent deviation from initial energy due for both schemes with variable Δt (Eq. (16)), and (b) shows how potential and kinetic energy change for both schemes (Eq. (17)).

$$\%\Delta K = \frac{K(\mathbf{v}) - H_0}{H_0} \times 100 \qquad \%\Delta U = \frac{U(\mathbf{x}) - H_0}{H_0} \times 100 \tag{17}$$

In addition to seeing the change in total energy, we can also see the change in potential and kinetic energy. Similarly Here it can be observed how after $t = t_c$, Euler's method begins to diverge from the initial amount of energy significantly, effectively increasing the rate of evolution of the plasma, as it can be noted from the premature increase in kinetic energy almost 1 second before RK4 at around $t \approx 9$.

Aside from confirming that RK4 is preferable in comparison to Euler's method, this analysis shows that the discontinuity in the kernel mentioned previously not only affects the definition and convergence of particles at the center of the vortices, but also greatly impacts the accuracy of the integration schemes used. All things considered, smoothing out these irregularities is an important issue that will be addressed in the next section.

4 Regularization

4.1 Regularized Green's Function and Electric Field Kernel

Given that we consider electrons to move in one dimension, we have that the kernel function $K(x, y)$ is discontinuous at the point $x = y$, as it can be seen from Eq. (7). Since the modeled plasma that is assumed to be collisionless, particles are subject to a large (discontinuous) change in the electric field direction when crossing over other particles. This effect is hard to capture accurately unless very small time steps are used. To solve this problem, a regularization parameter $\delta > 0$ is introduced to smooth the Green's function on Eq. (4). The regularized Green's function, denoted $g_\delta(x, y)$ is given by

$$g_\delta(x, y) = -\frac{c_\delta}{2}\sqrt{(x - y)^2 + \delta^2}. \tag{18}$$

From this, we get a similarly regularized kernel function $K_\delta(x, y)$:

$$K_\delta(x, y) = -\frac{c_\delta}{2}\frac{x - y}{\sqrt{(x - y)^2 + \delta^2}} + x - y, \quad c_\delta = \sqrt{1 + 4\delta^2}, \tag{19}$$

where the constant c_δ is introduced to ensure K has smooth derivatives. Analytically, Eqs. (**??**) and (19) approach their non-regularized counterparts from Eqs. (4), (7) respectively in the limit $\delta \to 0$. This is also illustrated in Figure 6.

As a result of regularization, the new system of ODE's is now given by

$$x_i''(t) = -\sum_{j=1}^{N} K_\delta(x_i(t), x_j(t))w_j. \tag{20}$$

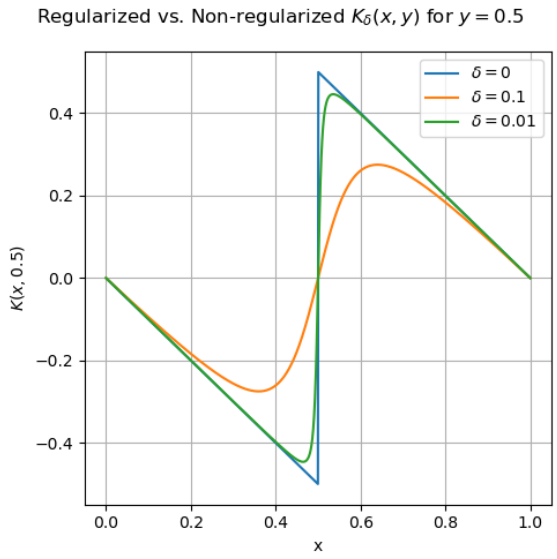

Figure 6: Regularized kernel function $K_\delta(x, 0.5)$ for different values of δ

4.2 Regularized Hamiltonian System

As a result of regularizing the electric field with Eq. (19), an alternative Hamiltonian $H_\delta(\mathbf{x}, \mathbf{v})$ is needed:

$$H_\delta(\mathbf{x}, \mathbf{v}) = \frac{1}{2}\sum_{i=1}^{N} v_i^2 + \sum_{i<j}\left[-\frac{c_\delta}{2}\sqrt{(x_i - x_j)^2 + \delta^2} + \frac{1}{2}(x_i - x_j)^2\right] w_j \tag{21}$$

Similarly to the non-regularized case, we can split this into kinetic and potential energy:

$$K_\delta(\mathbf{v}) = \frac{1}{2}\sum_{i=1}^{N} v_i^2, \quad U_\delta(\mathbf{x}) = \sum_{i<j}\left[-\frac{c_\delta}{2}\sqrt{(x_i - x_j)^2 + \delta^2} + \frac{1}{2}(x_i - x_j)^2\right] w_j \tag{22}$$

such that $H(\mathbf{x}, \mathbf{v}) = K_\delta(\mathbf{v}) + U_\delta(\mathbf{x})$.

To show that this is indeed a Hamiltonian system, consider a system of three particles in a regularized system, with phase space coordinates (x_1, v_1), (x_2, v_2), (x_3, v_3). Then the Hamiltonian from Eq. (21) is given by

$$\begin{aligned} H_\delta(\mathbf{x}, \mathbf{v}) = \frac{1}{2}(v_1^2 + v_2^2 + v_3^2) &+ \left[-\frac{c_\delta}{2}\sqrt{(x_1 - x_2)^2 + \delta^2} + \frac{1}{2}(x_1 - x_2)^2\right] w \\ &+ \left[-\frac{c_\delta}{2}\sqrt{(x_1 - x_3)^2 + \delta^2} + \frac{1}{2}(x_1 - x_3)^2\right] w + \left[-\frac{c_\delta}{2}\sqrt{(x_2 - x_3)^2 + \delta^2} + \frac{1}{2}(x_2 - x_3)^2\right] w \end{aligned} \tag{23}$$

First, we can see that for all three particles, this Hamiltonian expression in Eq. (21) satisfies the first equation from Eq. (13):

$$\frac{\partial H}{\partial v_1} = v_1 = x_1' \quad \frac{\partial H}{\partial v_2} = v_2 = x_2' \quad \frac{\partial H}{\partial v_3} = v_3 = x_3' \tag{24}$$

Similarly, the Hamiltonian expression from Eq. (21) also satisfies the second equation on Eq. (13):

$$\begin{aligned} -\frac{\partial H}{\partial x_1} &= -\left(-\frac{c_\delta}{2}\frac{x_1 - x_2}{\sqrt{(x_1 - x_2)^2 + \delta^2}} + x_1 - x_2\right) w - \left(-\frac{c_\delta}{2}\frac{x_1 - x_3}{\sqrt{(x_1 - x_3)^2 + \delta^2}} + x_1 - x_3\right) w \\ &= \left(\frac{c_\delta}{2}\frac{x_1 - x_2}{\sqrt{(x_1 - x_2)^2 + \delta^2}} - x_1 + x_2\right) w + \left(\frac{c_\delta}{2}\frac{x_1 - x_3}{\sqrt{(x_1 - x_3)^2 + \delta^2}} - x_1 + x_3\right) w \\ &= -K_\delta(x_1, x_2)w_2 - K_\delta(x_1, x_3)w_3 = v_1' \end{aligned} \tag{25}$$

$$
\begin{aligned}
-\frac{\partial H}{\partial x_2} &= -\left(-\frac{c_\delta}{2}\frac{-(x_1-x_2)}{\sqrt{(x_1-x_2)^2+\delta^2}} - (x_1-x_2)\right)w - \left(-\frac{c_\delta}{2}\frac{x_2-x_3}{\sqrt{(x_2-x_3)^2+\delta^2}} + x_2 - x_3\right)w \\
&= \left(\frac{c_\delta}{2}\frac{x_2-x_1}{\sqrt{(x_2-x_1)^2+\delta^2}} - x_2 + x_1\right)w + \left(\frac{c_\delta}{2}\frac{x_2-x_3}{\sqrt{(x_2-x_3)^2+\delta^2}} - x_2 + x_3\right)w \\
&= -K_\delta(x_2,x_1)w_1 - K_\delta(x_2,x_3)w_3 = v_2'
\end{aligned} \tag{26}
$$

$$
\begin{aligned}
-\frac{\partial H}{\partial x_3} &= -\left(-\frac{c_\delta}{2}\frac{-(x_1-x_3)}{\sqrt{(x_1-x_3)^2+\delta^2}} - (x_1-x_3)\right)w - \left(-\frac{c_\delta}{2}\frac{-(x_2-x_3)}{\sqrt{(x_2-x_3)^2+\delta^2}} - (x_2-x_3)\right)w \\
&= \left(\frac{c_\delta}{2}\frac{x_3-x_1}{\sqrt{(x_3-x_1)^2+\delta^2}} - x_3 + x_1\right)w + \left(\frac{c_\delta}{2}\frac{x_3-x_2}{\sqrt{(x_3-x_2)^2+\delta^2}} - x_3 + x_2\right)w \\
&= -K_\delta(x_3,x_1)w_1 - K_\delta(x_3,x_2)w_2 = v_3'
\end{aligned} \tag{27}
$$

A similar, yet more lengthy derivation can be done for a system of N particles.

4.3 Numerical Results

4.3.1 Qualitative Results

As mentioned before, one of the main issues that regularization seeks to solve is to increase definition and convergence at the center of the vortices formed in the plasma. This effect can be seen in Figure 7, where the previous vortex center is compared to a regularized one with $\delta = 0.01$. This regularization factor is rather small compared to the factors used in other simulations in this paper, but it is used to illustrate the effects of regularization while being a useful qualitative comparison to the non-regularized case.

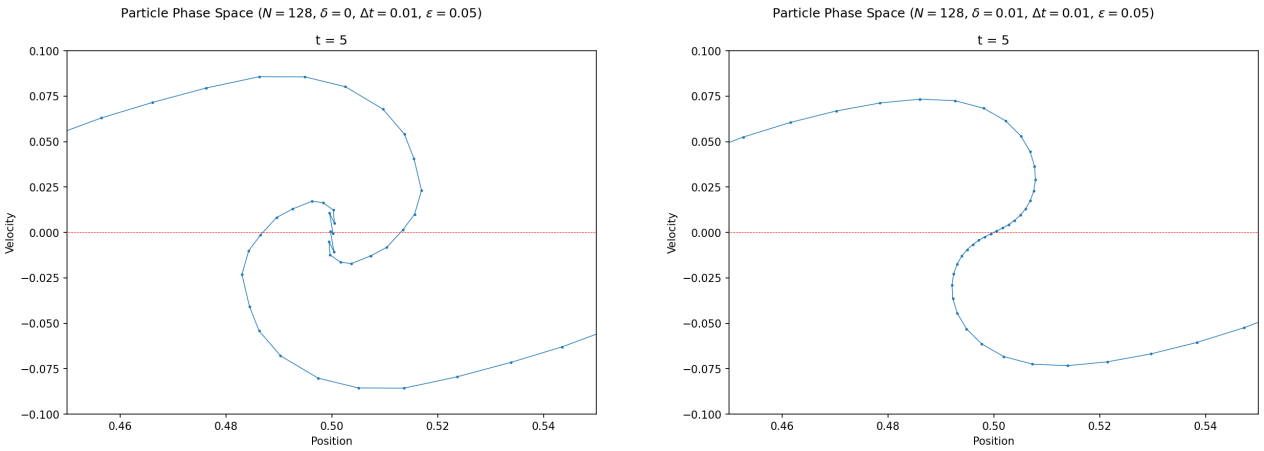

Figure 7: Effect of regularization on plasma, (a) without regularization, (b) regularization parameter $\delta = 0.01$.

One of the byproducts of the introduction of the regularization parameter is the "slowing down" of particles, particularly the ones close to the center of the vortex, as they now experience a smoother, more gradual change in acceleration when crossing over particles, rather than the rapid change from the discontinuous case, as illustrated in Figure 6. This can be better observed in Figure 8, where a regularized plasma is evolved up to $t = 10$. Comparing this evolution to its non-regularized counterpart from Figure 1, one can see that while regularization preserves larger features of the plasma, such as the curling around points of higher densities and the formation of "arms" that are transported to neighboring periods, the center of the vortices evolves at a slower rate than that of the non-regularized plasma. As expected, this effect is reduced as the regularization parameter δ is decreased. Refer to [1] in the Appendix for an animation of the evolution of the regularized plasma.

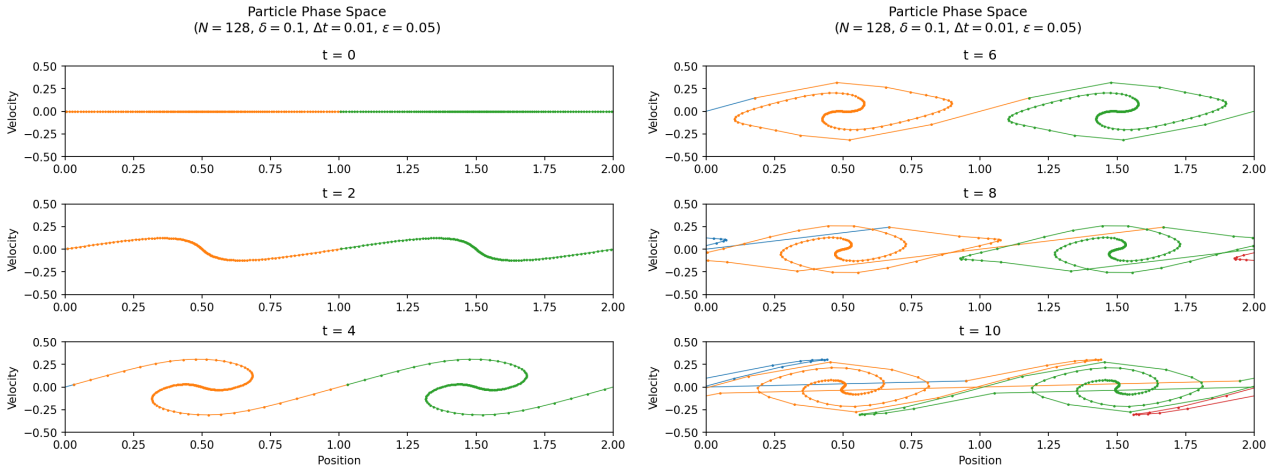

Figure 8: Evolution of regularized plasma with $\delta = 0.1$

4.3.2 Error Analysis

Another area of interest with regularization is its effect on rate of convergence for both integration schemes considered, as it removes discontinuities that may have impacted these schemes' performance. All of these calculations use an equation similar to Eq. (16):

$$\%\Delta E_\delta = \frac{|H_\delta(\mathbf{x}, \mathbf{v}) - H_{\delta,0}|}{H_{\delta,0}} \times 100 \quad H_{\delta,0} = H_\delta(\mathbf{x}(0), \mathbf{v}(0)) \tag{28}$$

First, Figure 9 exhibits how error is affected by different time steps on the regularized plasma with $\delta = 0.1$, both for Euler's Method and RK4. Similarly to the results from the non-regularized system, we can see that there is a proportional decrease in error due as time step size decreases for Euler's method. However, for RK4 there is little to no improvement in error as time step size decreases, opposite to what was observed in the non-regularized system in Figure 5. Regardless, RK4 still outperforms Euler's method for the time step sizes considered. This could be attributed to the fact that being a fourth-order system, eliminating discontinuities in the first derivative of the governing ODE's is not enough to guarantee fourth-order convergence. However, it is unclear why discontinuous set of ODE's from the non-regularized case outperforms the regularized system for equal time step sizes, and further analysis is required. Another possibility may be that the regularized system experiences heating, and the smoothness introduced by the regularization causes the RK4 scheme to converge very rapidly, for which further analysis is required. This may also open the door for exploring alternate regularization functions.

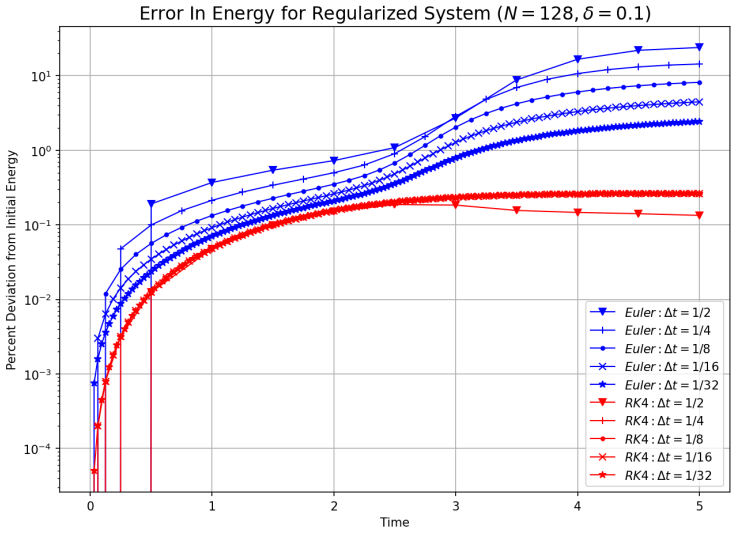

Figure 9: Error (Eq. (28) in energy due to regularized Euler's method and RK4 for $\delta = 0.1$

A better comparison between the non-regularized and regularized plasma can be observed in Figure 10a for Euler's method and Figure 10b for RK4. On the former, we can see that regularization causes an overall decrease in error for each time step size, while the decrease in error seems to be roughly similar. Additionally, while there is an increase in error after particle collision in the regularized case at approximately $t = 2.5$, the increase in error is both more gradual and of smaller overall magnitude compared to the non-regularized system. For RK4, as noted earlier, higher-order convergence is absent for the entirety of the time interval considered, whereas it could be observed before particle collision occurred for the non-regularized system. Quantitatively, regularized RK4 seems to perform about an order of magnitude worse, as error seems to be the largest in the order of tenths of a percent. However, Figure 11 initially suggests that this error is proportional to the regularization parameter δ, as it illustrates how decreasing δ causes the error to decrease as well, though further analysis incorporating varying time step sizes Δt and number of particles N is required here to reach a stronger conclusion.

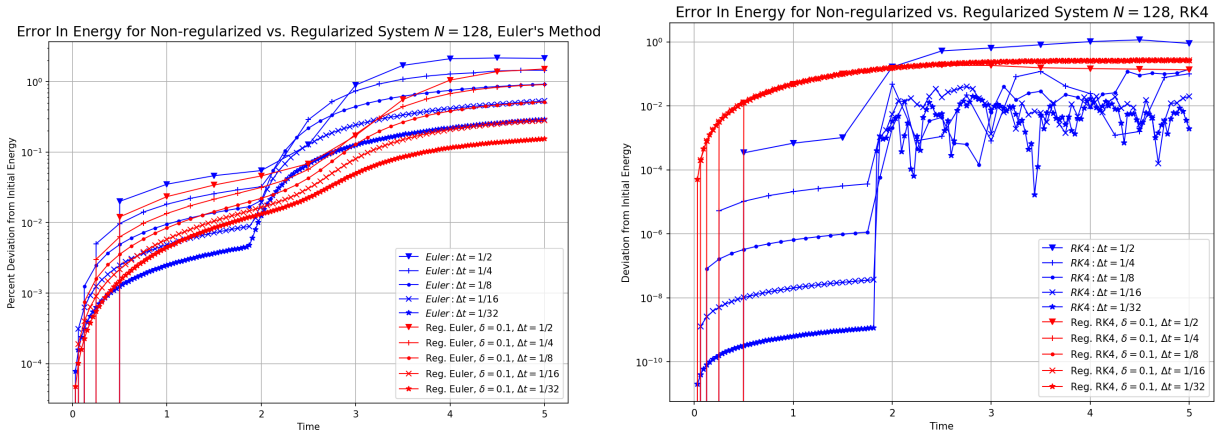

Figure 10: Error comparison between non-regularized and regularized plasma evolved with (a) Euler's Method and (b) RK4

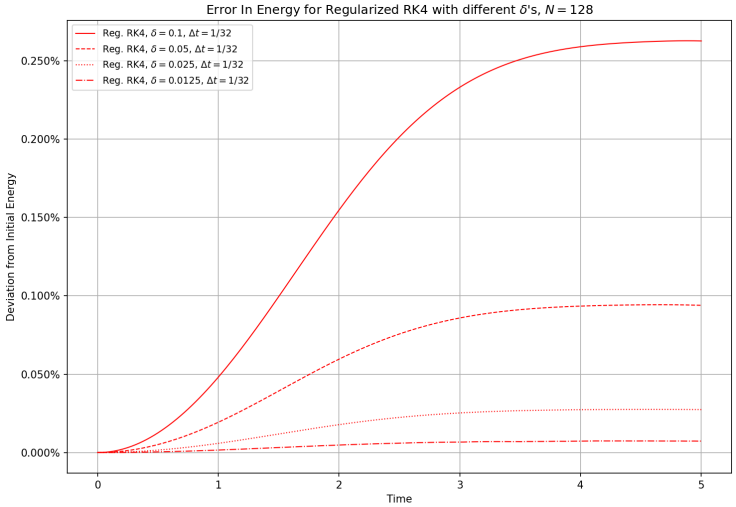

Figure 11: Effect of error due to different regularization parameters δ for RK4

5 Adaptive Particle Insertion

5.1 Particle Insertion Scheme

As discussed previously, one of the biggest drawbacks of the current implementation is the loss of definition as the plasma evolves and particles are convected away from each other. To amend this, the following adaptive particle

insertion scheme is proposed. Instead of discretizing the plasma into N particles placed at the midpoints of the N intervals (see Figure 12a), this scheme uses two kinds of particles: passive and active particles (see Figure 12b). Active particles are initially placed at the midpoints of the intervals, and it is only these particles that contribute to the overall electric field responsible for the evolution of the plasma. On the other hand, passive particles are placed at the endpoints of the discretized intervals. These particles have no contribution to the electric field, and are transported by the flow along with other particles.

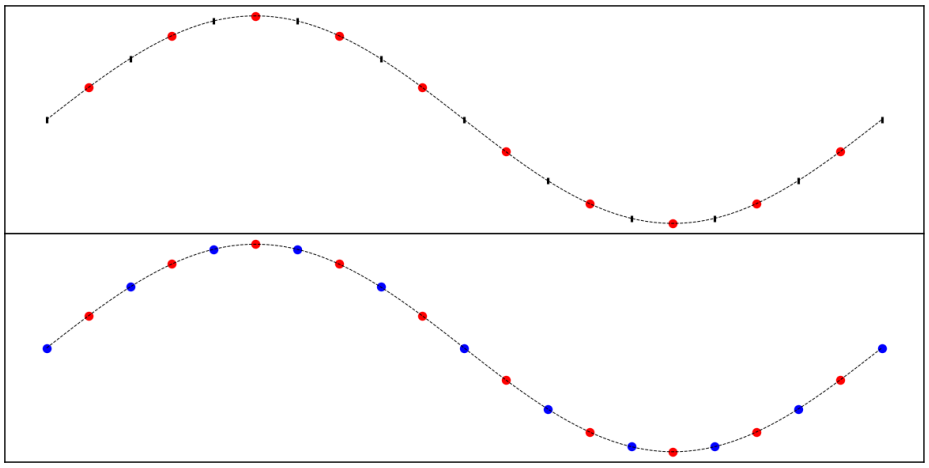

Figure 12: Different particle discretization schemes: (a) previously proposed schemes with only active particles (red) at the midpoints of the intervals, (b) new scheme with passive (blue) particles at the endpoints of the intervals.

An additional threshold parameter, d_1 is introduced. As the plasma evolves, the length of the discretized intervals, i.e. the total distance between adjacent pairs of passive particles, is tracked. If the distance between adjacent passive particles exceeds the threshold value d_1, particle insertion is triggered. Let p_1, p_2, p_3 denote the three particles in the interval, with p_1 and p_3 being the passive particles at the ends of the interval and p_2 being the active particle at the midpoint of the interval, as depicted in Figure 13a. The interval is then split in two and p_2 is converted to a passive particle. Two new particles, p_4 and p_5 are introduced. First, p_4 is inserted between particles p_1 and p_2, with Lagrangian coordinate α taken as the average of the coordinates of p_1 and p_2. Similarly, p_5 is inserted between p_2 and p_3, with its Lagrangian coordinate calculated in the same way. Using the positions and velocities of p_1, p_2, and p_3, the new positions and velocities of p_4 and p_5 are calculated using quadratic interpolation with respect to their Lagrangian coordinates. This process is illustrated in Figure 13b. Additional information such as number of periods travelled is also updated on the new particles.

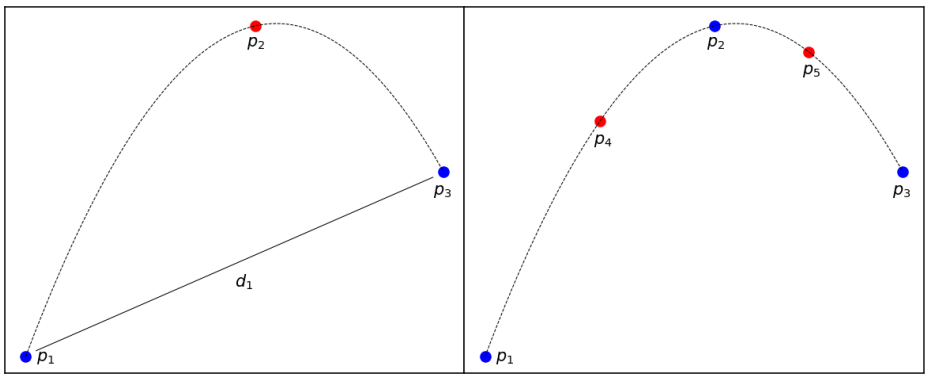

Figure 13: Adaptive particle insertion (a) before insertion, where distance between passive particles exceeds threshold distance d_1 and (b) after particle insertion occurs.

5.2 Numerical Results

The introduction of particle insertion brings in a significant increase in definition as the plasma evolves. This can be seen in Figure 14, where a plasma of initially $N_0 = 200$ particles is evolved with an insertion parameter $\delta_1 = 0.05$ until $t = 20$ when $N = 7152$. Here, each different color represents plasma from a different starting interval, for a total of 8 different intervals. Unlike previous simulations, detail is now preserved on the edges of the periodic intervals, where the plasma is stretched and compressed as neighboring periods are transported along. This detail can be better seen in larger plots of the final stage of the plasma in Figure 15, where the plasma is plotted both with connecting lines (Figure 15a) and without connecting lines (Figure 15b). It is worth noting that even without the connecting lines, the overall structure of the plasma can still be observed. In addition to this, Figure 16 focuses on the detail that arises at the boundary between two periods. Refer to [2] in the Appendix for an animation of the evolution of the regularized plasma.

With a variable number of particles, a function of energy equivalent to Eqs. (13) and (21) is needed to assess the accuracy of the simulations with the addition of particle insertion.

6 Summary

The proposed Lagrangian particle method to simulate 1D cold electrostatic plasma with the addition of regularization and adaptive particle insertion is a promising alternative to existing PIC methods in terms of preservation of detail as the plasma evolves and develops complex features. Still, some aspects of regularization, such as its effect on error in conserved energy for different N and Δt and its quantitative effect on the evolution rate of the plasma should be studied more extensively, as well as exploring alternate regularized electric fields that may preserve higher order convergence in used integration schemes. Eventually, this method should be extended to investigate other types of distributions, such as multiple-stream instabilities and warm distributions. Nevertheless, there are still several things left to be investigated regarding cold, electrostatic 1D plasma with the current method, such as tracking charge transport across periods, studying the dynamics of potential and kinetic energies and their relationships to overall features of the plasma, and looking into whether phenomena such as Landau dampening are present.

References

[Mit+19] Matthew S. Mitchell et al. "Efficient Fourier basis particle simulation". In: *Journal of Computational Physics* 396 (2019), pp. 837–847. ISSN: 0021-9991. DOI: https://doi.org/10.1016/j.jcp.2019.07.023. URL: https://www.sciencedirect.com/science/article/pii/S002199911930508X.

[STK23] Ryan Sandberg, Alexander G. R. Thomas, and Robert Krasny. "A Forward Adaptively Refined and Regularized Semi-Lagrangian Integral GPU- and Hierarchical Tree-code-accelerated method for the Vlasov-Poisson system." In: *in preparation* (2023).

A Simulation Animations

1. Plasma simulation without particle insertion: https://youtu.be/6aweVxwhNic
2. Plasma simulation with particle insertion: https://youtu.be/ioqL1jhSXUc

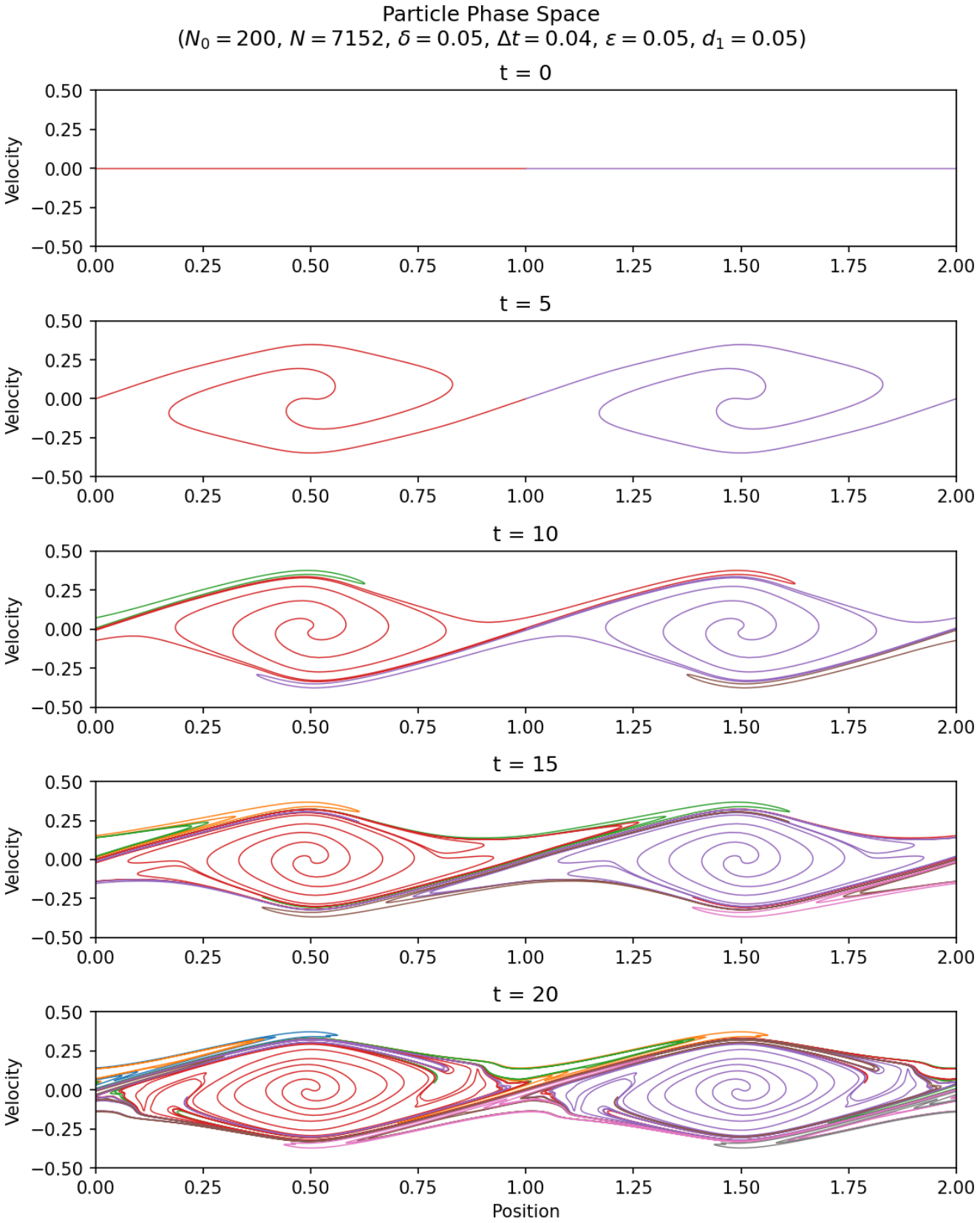

Figure 14: Evolution of plasma with particle insertion for $t = 20$ with parameter $d_1 = 0.05$

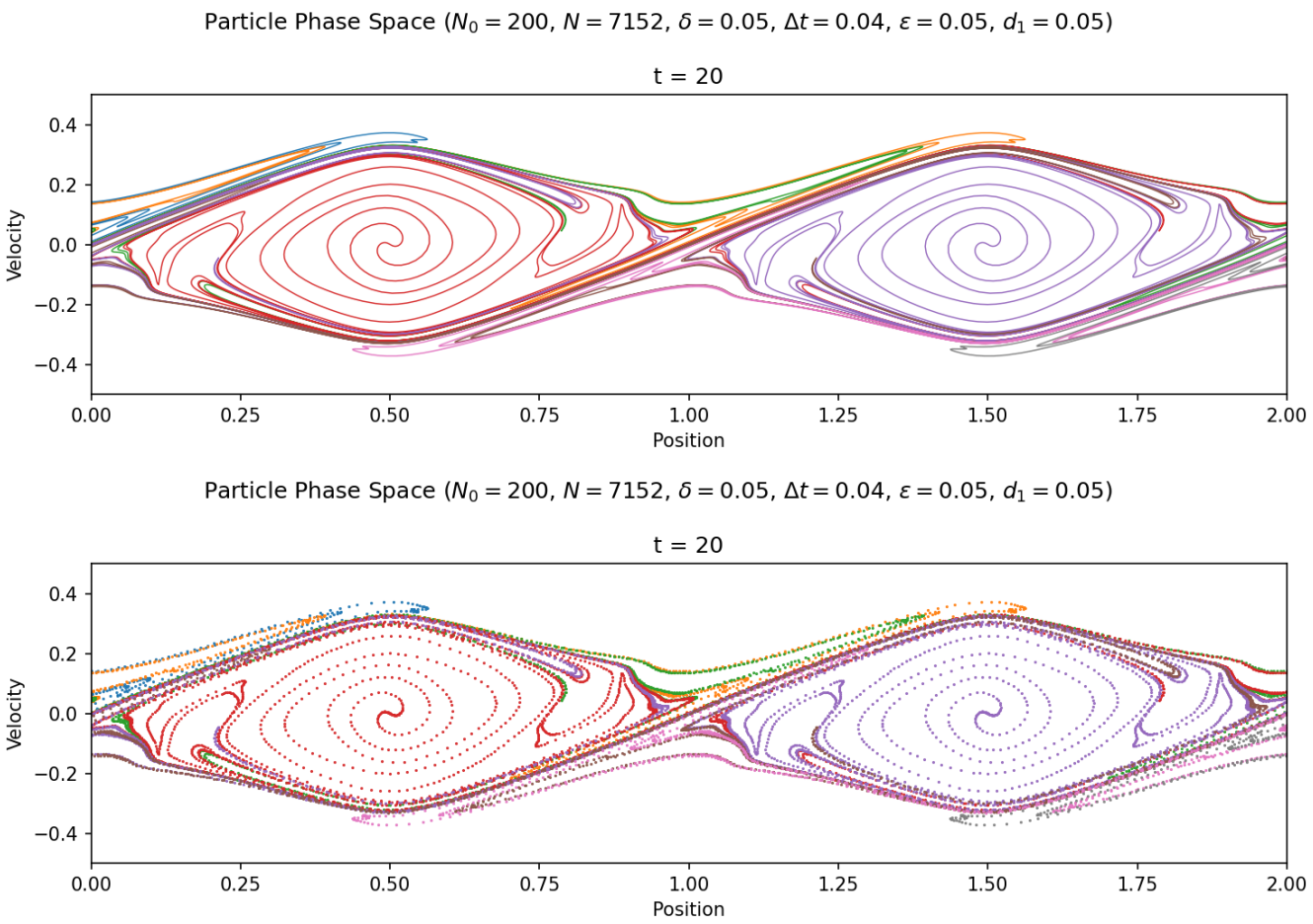

Figure 15: Plasma evolved with particle insertion $d_1 = 0.05$ at $t = 20$ (a) with connecting lines and (b) without connecting lines

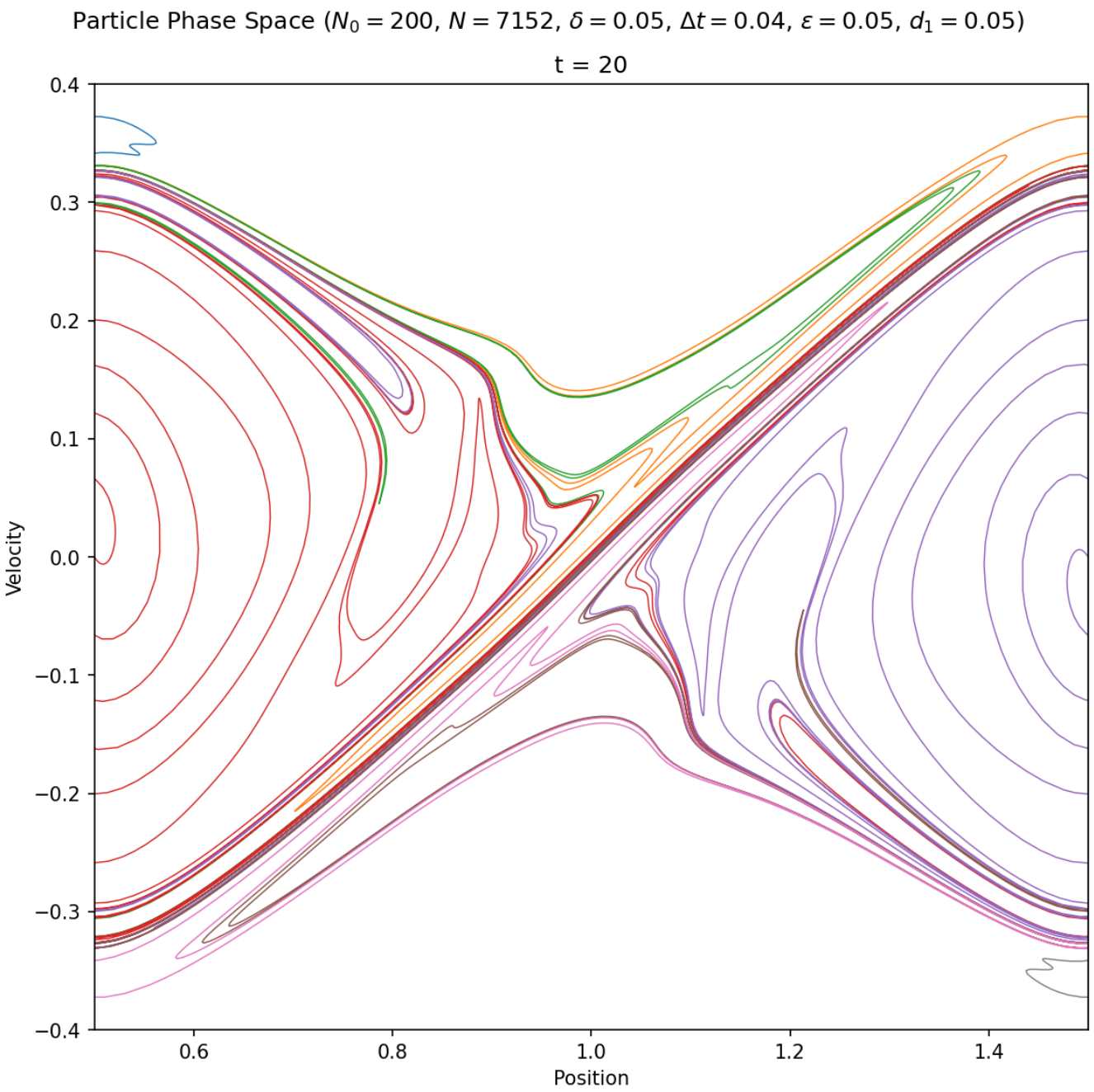

Figure 16: Expanded plot of plasma with particle insertion in region between two periods at $t = 20$